Draft version August 10, 2023
Typeset using LaTeX **preprint** style in AASTeX631

Beam Mapping of LWA using Pulsar Gating

Akshatha K Vydula [1], Judd D Bowman,[1] and Daniel C Jacobs[1]

[1] *School of Earth and Space Exploration, Arizona State University ,Tempe AZ USA 85281*

ABSTRACT

We plan to adopt the pulsar gating method of beam calibration for OVRO-LWA. As a preliminary test, we use the Very Large Array (VLA) to track a pulsar and simultaneously let it drift through the beam of the co-located LWA-1 station near Socorro, New Mexico. The difference between the on-pulse and off-pulse periods of the observations will correspond to a stable, reasonably known, flux of the pulse, providing an absolute flux reference that is not contaminated by diffuse background sky emission. We were able to verify the system equivalent flux density (SEFD) of LWA-1 to be 4680 Jy at 75 MHz by detecting the pulsar B1133+16 with an SNR of 9.02 dB using the eLWA binning correlator, which falls within the expected $11.69^{+1.76}_{-3.02}$ dB. As an additional test, we also used PRESTO to detect the pulsar with an SNR of 10.93 dB. We plan to use this method to also measure SEFD of VLA, which is poorly known at the 4-meter wavelengths. We will then use cross-correlations of the pulsar signal between the two telescopes to measure the LWA-1 average antenna beam response along the path of the pulsar.

Keywords: pulsar holography - beam mapping - epoch of reionization - radio interferometry

1. INTRODUCTION

The Universe as we now know and understand was filled with dense, ionized matter for the first 350,000 years (Pritchard & Loeb 2012). As it expanded, the matter cooled leading to electron and protons coming together to form neutral hydrogen in what is called the Dark Ages era, where there was no light. Gravity brought the matter together to form some of the first stars and Galaxies, in the Cosmic Dawn era. The UV radiation from the first stars and Galaxies caused decoupling of neutral hydrogen gas temperature and the Cosmic Microwave Background (CMB) temperature leading to cooling of hydrogen gas. The X-ray radiation heats the gas and eventually the UV radiation takes over and re-ionizes the neutral hydrogen in an era called the Epoch of Reionization(EoR).

Figure 1 shows a schematic of various phase transitions of the Universe.

The electron in the neutral hydrogen undergoes a hyperfine spin-flip transition from two parallel spin states to a more stable parallel and an anti-parallel spin state causing emission of radiation at a rest wavelength of 21 cm (and rest frequency of 1421 MHz). The likelihood of 21 cm line transition is very low, but the abundance of hydrogen in the Universe makes this an observable signal (Liu & Shaw 2020). This line from EoR is a highly redshifted ($\sim z = 6-50$), (Thomas et al. 2009; Furlanetto et al. 2006), currently observable at much lower frequency in radio frequency range of 50-200 MHz.

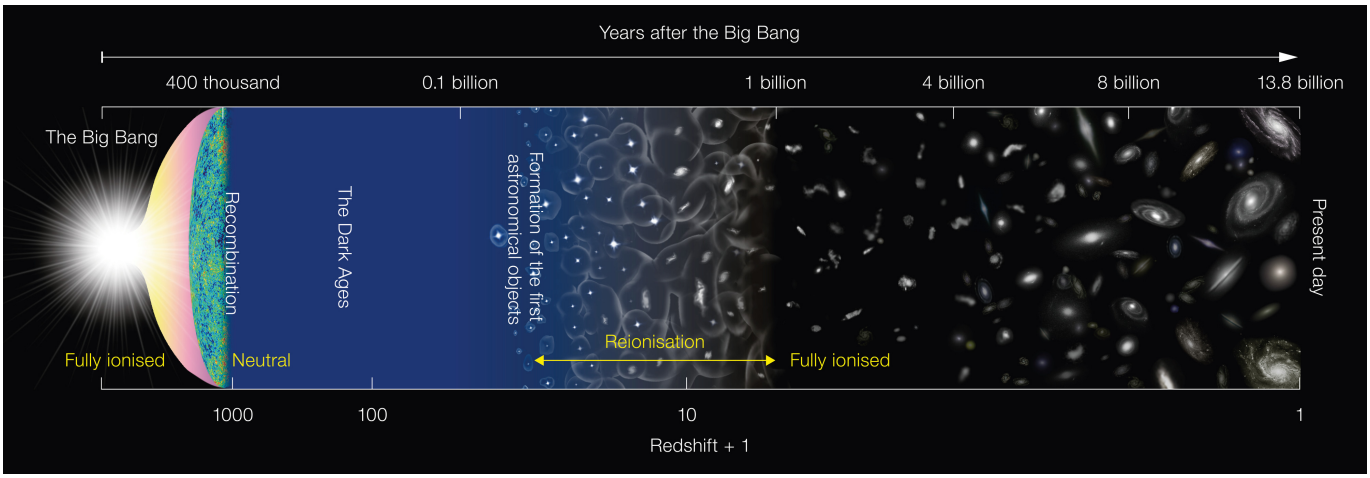

Figure 1. Timeline of evolution of Universe showing various phases starting from the Big Bang, Dark Ages, Cosmic Dawn, Epoch of Reionization and leading up to present day local structures in the Universe. *(Source: NAOJ, designed for the press release of Inoue et al. (2016))*

The redshifted 21 cm signal is a direct probe of studying Cosmic Dawn and EoR, but is a weak transition and requires bright radio sources at high redshifts (Ciardi et al. 2013), making the detection very challenging. Observation in this frequency range is also extremely challenging due to terrestrial radio frequency interference (RFI), synchrotron emission, free-free emission at low frequencies (Santos et al. 2005) and contamination from Milkyway which are orders of magnitude brighter than the signal of interest (Bernardi et al. 2009; Spinelli et al. 2018). Due to these challenges, currently, two significant observational gaps remain in understanding the evolution of the Universe, the Cosmic Dark ages and the formation of the first luminous stars and galaxies during the era of Epoch of Reionization (Furlanetto et al. 2006).

A precise modelling of foregrounds, RFI and instrumental contamination is necessary, which makes this observation an engineering challenge. Studying the redshifted 21 cm signal from these epochs thus constitutes the next frontier of observational cosmology, allowing direct study of the characteristics of the first stars and Galaxies.

Various research teams around the world are actively working to make this observation. LOw Frequency ARray (LOFAR, Yatawatta et al. (2013)), Murchison Widefield Array (MWA, Barry et al. (2019)), Precision Array for Probing the Epoch of Reionization (PAPER, Parsons et al. (2014)), hydrogen Epoch of Reionization Array (HERA, Abdurashidova et al. (2022)) and Square Kilometre Array (SKA, Koopmans et al. (2015)) are radio interferometers performing 21 cm power spectrum measurements. EDGES (Bowman et al. 2018), Shaped Antenna measurement of the background RAdio Spectrum (SARAS, Nambissan T et al. (2021); Singh et al. (2022)) and Large-aperture Experiment to Detect the Dark Age (LEDA, Price et al. (2018)) are single antenna experiments, measuring the all-sky global averaged redshifted 21 cm signal. There are also significant efforts in space-based measurements using currently in orbit James Webb Space Telescope (JWST, Windhorst et al. (2006)) and future experiments such as Farside Array for Radio Science Investigations of the Darkages and Exoplanets (FARSIDE, Burns et al. (2019a, 2021)), Probing ReionizATion of the Universe using Signal from Hydrogen (PRATUSH, [Mayuri Rao's talk at the 4th Global 21cm workshop, no citations yet]) and EDGES in Space [no citations yet].

As a result of technological advancements in understanding of the instrument and with better simulations and modelling of the sky, there have been significant improvements in upper limits of 21 cm power spectrum measurements. Barry et al. (2021) give a comparative study of various radio interferometers with an improvement in upper limits by an order of 6 magnitude in the EoR window over the past decade. But a confident measurement is still due and requires improving the instrument systematics.

In radio interferometers the frequency dependent primary beam patterns are one of the significant contributor of these systematics, thus accurate modeling and calibration of the primary beam is necessary. Traditionally, calibration is done by mapping all the known point sources in the field of view. But this is a complicated procedure as it requires achieving a very high angular resolution to distinguish faint sources in the beam. Some of these radio sources are extended in angular scales with jets and lobes which cannot be accounted for in this method of calibration. Beyond this, it is worth noting that the catalogs are incomplete and contain uncertainties, which will lead to calibration errors.

The Owens Valley Long Wavelength Array (OVRO-LWA) is a low-frequency radio interferometer located in Owens Valley, California with the primary goals of studying the high redshift HI 21cm signal and radio emission from exoplanet and stellar systems (Anderson et al. 2018). In this project, we attempt to address the short comings in beam calibration by developing a beam mapping method by using bright pulsars. We use a known, well-understood antenna to track a pulsar while it drifts through LWA's beam.

For initial development and testing of the proposed method, we use simultaneous observations from Very Large Array (VLA) and two LWA stations in New Mexico (LWA-1, close to VLA center and LWA-SV, $\sim$ 80 km North-East of VLA center). After demonstrating the proof of concept, we plan to use 40 m dish at OVRO with an LWA feed installed at it's prime focus, to make the beam calibration measurements of OVRO-LWA.

2. PROPOSED METHODOLOGY

The initial test will involve simultaneous observation of a bright pulsar using VLA and LWA, where the source will drift through the latter while being tracked by the former. Starting with the visibility equation for a baseline involving a VLA antenna with antenna gain g_i and a beam $B_i(\hat{s})$ and one of the beamformed LWA stations with antenna gain g_L and beam $B_L(\hat{s})$:

$$\begin{aligned} V_{iL} =& g_i g_L \Big[B_L(\hat{s}) B_i(\hat{s}) I_P(t) e^{-\vec{\mathbf{b}}_{iL}\hat{s}\nu/c + \phi_i + \phi_L + \delta_i \nu} \\ &+ \int B_L(\hat{s}) B_i(\hat{s}) I_s e^{-\vec{\mathbf{b}}_{iL}\hat{s}\nu/c + \phi_i + \phi_L + \delta s + \delta_i \nu} \Big] \end{aligned} \tag{1}$$

where, $I_P(t)$ is the pulsar flux, ϕ represents phase of each antenna, $\delta_i \nu$ is the cable delay and second term of the equation 1 is the contribution from the sky consisting of sources $I(s)$. Since the flux from these sources (rest of the sky) will fairly remain unchanged in the timescales of period of a pulsar, we can remove this flux contribution simply by subtracting the fluxes when the pulsar peaks (on period) and when it does not (off period), essentially giving a stable known pulsar flux. So we have,

$$\begin{aligned} V_{iL,on} - V_{iL,off} = \Delta V_{iL} = \\ g_i g_L B_i(\hat{s}) B_L(\hat{s}) I_P(t) e^{-\vec{\mathbf{b}}_{iL}\hat{s}\nu/c + \phi_i + \phi_L + \delta_i \nu} \end{aligned} \tag{2}$$

$B_i(\hat{s})$ reduces to unity for source tracking VLA antennas and the on and off time pulsar flux $I_P(t)$ can be calculated by solving for $g_i, \phi_i, \delta_i\nu$ in multiple inter-VLA baselines using calibrator source, I_C,

$$V_{ij}^{cal} = g_i g_j I_C e^{-\vec{\mathbf{b}}_{ij}\hat{s}\nu/c+\phi_i+\phi_j+\delta_i\nu} \tag{3}$$

We get N such measurements from all the inter-VLA baselines. A summation over all of them can be used as a single VLA station of gain g_V.

$$\begin{aligned} V_V^{cal} =& \frac{I_C}{N}\sum_{i\neq j}^{all} g_i g_j e^{-\vec{\mathbf{b}}_{ij}\hat{s}\nu/c+\phi_i+\phi_j+\delta_i\nu} \\ =& g_V^2 I_C \end{aligned} \tag{4}$$

Assuming the complex gain of LWA-1 remains stable as a function of time, we can now use the known pulsar flux $I_P(t)$ in the visibility of a VLA-LWA baseline to calculate the only unknown parameter $B_L(\hat{s})$, beam of LWA.

$$V_{VL}^P = g_V g_L B_L(\hat{s}) I_p(t) e^{-\vec{\mathbf{b}}_{VL}\hat{s}\nu/c+\phi_V+\phi_L+\delta_{VL}\nu} \tag{5}$$

We propose using a bandpass calibrator and two gain calibrators, the primary being a calibrator source to solve for VLA antenna gain and phases and the secondary calibrator source for testing the stability of gain solutions. Applying these calibration solutions to the pulsar flux and subtracting the visibilities during the pulsar on and off periods gives a stable known pulsar flux within the time scales of pulsar period. This can be used to calculate the beam pattern of the LWA from visibilities involving both VLA and LWA antennas in the baselines. We note that this measurement holds good within the reasonable assumption of stable gain of LWA for drift scans. We also note that this method also gives the beam patterns at limited declinations of selected pulsars and could potentially require other bright sources for beam mapping the full field of view.

A similar method has been proposed (Newburgh et al. 2014) and adopted for beam calibration of Canadian Hydrogen Intensity Mapping Experiment (CHIME) (Berger et al. 2016). Using John A. Galt 26 m telescope, 7 bright point sources were mapped throughout the frequency band of CHIME. They showed that a longer integration time is necessary for better SNR and other methods of beam mapping could be helpful along with pulsar holography to realistically map the CHIME beam.

3. OBSERVATION AND DATA ANALYSIS

3.1. *Sensitivity Analysis*

Sensitivity of a radio antenna is defined as it's ability to detect the weakest radio source (Taylor et al. 1999). To confidently select and detect a pulsar, we first started with the sensitivity of VLA and LWA systems in three different modes of correlations. The three modes are auto-correlation of an LWA system, cross-correlation between a single VLA dish with the LWA system and cross-correlation between the full VLA array with LWA system. We calculated a sensitivities in each of these correlation modes which allows us to predict the signal-to-noise ratio (SNR) of selected pulsars in each of these modes.

Sensitivity for a two antenna system can be defined as:

$$\Delta S_{ij} = \frac{1}{\eta_s}\sqrt{\frac{\mathrm{SEFD}_i \mathrm{SEFD}_j}{2\Delta\nu\tau_{acc}}} \tag{6}$$

where, η_s is the product of two independent antenna efficiency (typically unity for dipoles), $\Delta\nu$ is the spectral bandwidth and τ_{acc} is the correlator accumulation time. System Equivalent Flux Density (SEFD) is an antenna property that represents the system temperature, defined as the flux density of a source that delivers the same amount of power as the system temperature (Taylor et al. 1999).

$$\text{SEFD} = \frac{T_{sys}}{K}, K = \frac{\eta_a A}{2k_B} \tag{7}$$

where, T_{sys} is system temperature and K is a measure of antenna performance calculated using the area of the antenna and antenna efficiency. SEFD of a single LWA dipole antenna is calculated to be 1 MJy (Ellingson 2011), and that of a single VLA dish is 50 kJy (NRAO-VLA Observing manual 2021). Equation 6 gives the sensitivity of a two antenna system. For a spectral bandwidth of 8 MHz and integration time of 200 s, we get a sensitivity of 3.952 Jy. The SEFD of 256 element LWA array is estimated to be 4680 Jy at 75 MHz (LWA-1 Observing Manual 2012), which improves the sensitivity to 0.2704 Jy. For an interferometric system of N identical antennas, sensitivity can be simply calculated using

$$\Delta S = \frac{SEFD}{\eta_a \sqrt{N(N-1)\Delta\nu\tau_{acc}}} \tag{8}$$

For a full VLA array consisting of 26 dishes, and a spectral bandwidth of 8 MHz and integration time of 20 s, we get a sensitivity of 0.1550 Jy. Table 1 summarizes the sensitivity estimation in all three correlation modes.

Correlation mode	$\tau_{acc}(s)$	Sensitivity (Jy)
Single LWA dipole & Single VLA dish	200	3.952
256 element LWA & Single VLA dish	200	0.270
256 element LWA & 26 VLA dishes	20	0.155

Table 1. Sensitivity estimation of LWA and VLA in three different correlation modes with spectral bandwidth of 8 MHz.

We use these sensitivity estimations to select bright pulsars observable by both VLA and LWA.

3.2. *Candidate selection and Observation*

We used the Australian Telescope National Facility (ATNF) pulsar catalogue (Manchester et al. 2005) to list all the pulsars brighter than 1 Jy at 80 MHz. Of the 11 shortlisted pulsars, we need the pulsar to be above the horizon in the daytime (to fit into fixed VLA testing time), close to zenith. With the high gain in narrow beams, the emissions from the Sun will be significantly attenuated, so no strategies were applied to mitigate this effect. The most optimum candidate was the pulsar $B1133+16$, with source flux of 4.730 ± 2.370 Jy at 80 MHz and RA: 11:36:03.1198, DEC: +15:51:14.183. B1133+16 is a radio pulsar with double pulse profile and dispersion measure of 4.844 ± 0.002 (Karuppusamy et al. 2011). B1133+16 has also been detected using LWA archival

data with reported pulse period of 1.1879 s and mean flux density of 4.73 ± 2.37 Jy at 79.2 MHz (Stovall et al. 2015).

We used NRAO's Observation Preparation Tool (OPT) portal to schedule and record the observation in eLWA observing mode (eLWA Observing Manual 2021) with VLA in B configuration. The eLWA mode of observation records data from individual VLA antennas and from two LWA stations (LWA-1 and LWA-SV) in a 8 MHz bandwidth centered at 76 MHz. The correlations were performed offline using the raw voltage streams. We selected Cygnus-A for band-pass calibration, 3C295 as primary gain calibrator and 3C196 as a secondary gain calibrator. The target pulsar was observed for $\sim$ 14 minutes. The dishes can steer from -85^o to +445^o, changing azimuth at the rate of 40 deg/min. The first dummy scan should therefore be at least 9 min to account for the worst case scenario, to be able to point to the source. Longest it can take is about 13 min 40 sec, but it is unlikely in most cases, thus the conservatively set slew time was 9 min. We recorded the data on September 20, 2021 in the LST window of 13.5 h to 15 hr. Table 3 gives the observation sequence and time on each source involving the target pulsar, band-pass, primary and secondary calibrators.

3.3. *Data Reduction and Analysis*

To confidently do the beam mapping measurements, we first compared the results of pulsar detection from the binning correlator with the results from `PRESTO`. Binning correlator is an offline correlator developed for processing raw LWA-1 data, synthesize a filter bank, and apply incoherent de-dispersion to the data suitable for pulsar detections (Dowell et al. 2012). `PRESTO` (PulsaR Exploration and Search TOolkit) is a pulsar search and analysis software designed to detect millisecond pulsars.

3.3.1. *Pulsar detection using `PRESTO`*

We used `PRESTO`[1] (Ransom et al. 2003) on LWA-1 auto-correlations for detecting the pulsar. Using the raw voltage stream and applying RA, DEC and DM from the pulsar `psrfits` file was created with 64 profile bins. `rfifind` was used to create RFI masks, Figure 2 shows the RFI mask for LWA-1 data.

The generated RFI mask, pulsar period of 1.18 s were applied to fold the data using `prepfold`. `PRESTO` fits the data with the input pulse period and DM parameters and measures the best-fit parameters as a reduced χ^2 against a random noise model. We saw a strong 18.1σ detection and the waterfall of the detection also had a glitch at $\sim$61 s which impacted the reduced χ^2, so the analysis was re-done by conservatively excluding the first 100 s of the data. The updated data had a 14.9σ detection as shown in Figure 9. The phased pulse profile shows a double peak pulsar as expected. The middle plot shows the frequency waterfall diagram and best fit DM against reduced χ^2. Rightmost plots show the best-fit period (P), derivative of the period($P - dot$) and a $P - vs - P - dot$ of B1133+16.

`PRESTO` reports the pulse profile in powers with the mean noise level of unity. Therefore to calculate the SNR of the detection, the square root of the reported powers was calculated to get the amplitude values followed by subtracting 1 to get the pulse profile. We found that the pulsar peak was 4 bins wide in a 64 profile bin folding and we report an SNR of 10.93 dB detection of the pulsar B1133+16.

3.3.2. *Pulsar detection using binning correlator*

[1] https://github.com/scottransom/presto

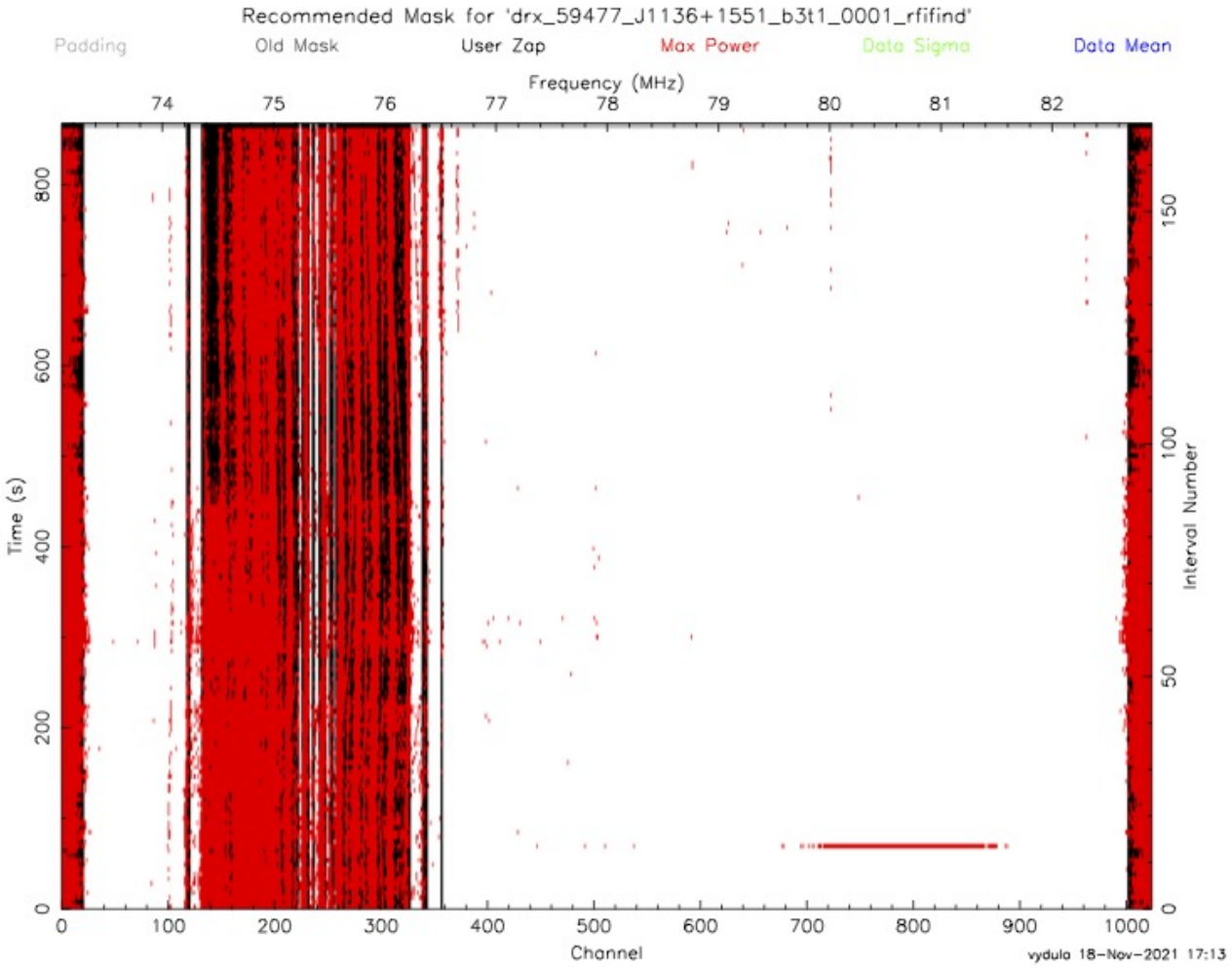

Figure 2. RFI mask generated using `PRESTO`'s `rfifind` module for B1133+16 data recorded by LWA-1.

The data from the test observation was correlated offline using eLWA correlator[2] and was stored in the `hercules` cluster at University of New Mexico. The correlation products, stored as `FITS-IDI` files, were transferred to `enterprise` at ASU for all the analysis. `CASA`'s `importfitsidi` was used to convert the files to measurement sets. We note that there are some `FITS-IDI` file reader issues that incorrectly transfer antenna locations, source IDs and phase centers among others when writing the measurement sets. This potentially needs a patch-up script for gain calibration stability analysis.

Figure 3 shows the waterfall of LWA-1 auto-correlation products. The binning correlator handles data in 10 ms sub-integration bins. To have the phase lined up to an integer multiple of the pulse period, the number of profile bins was set to 119 (closest to 1.1879 s), resulting in an integration time of 3.247 s.

Figure 4 shows the waterfall plot of the auto-correlation products from the binning correlator and it is clear from the plot that the glitch described in Section 3.3.1 is also evident here at ∼61 s.

[2] https://github.com/lwa-project/eLWA

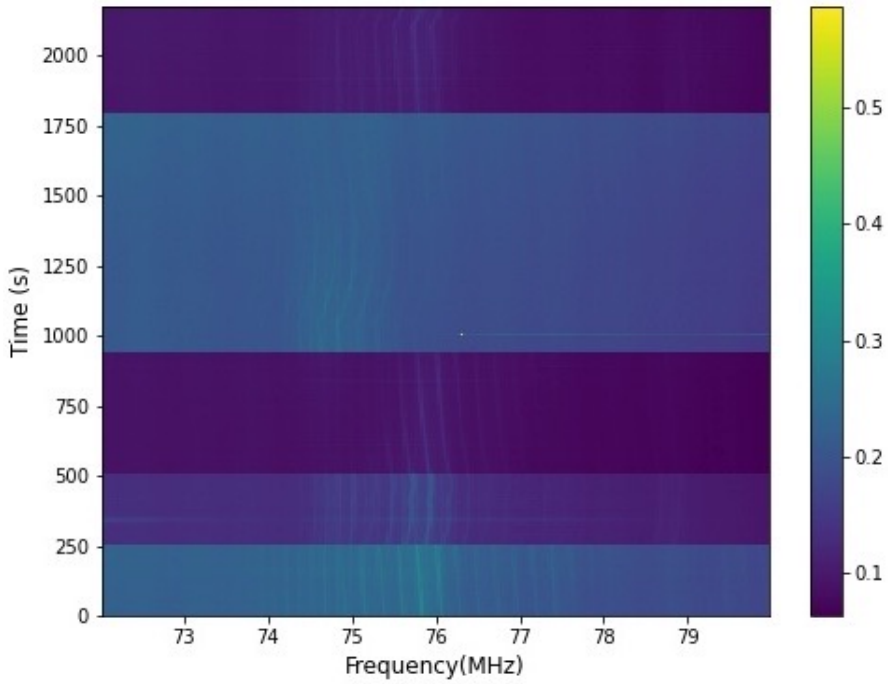

Figure 3. Auto-correlation products of LWA-1 for the full observation, involving Cygnus-A, 3C196, 3C295 and B1133+16.

Figure 5 shows the glitch, most likely caused due to a short time burst of an instrumental artifact, plotted against some of the normal time bins for reference. This time bin was flagged appropriately before doing a median subtraction and averaging across time to obtain a pulse profile as shoown in Figure 7.

The analysis was repeated in the frequency axis and a broadband RFI was seen in the frequency range of 74-75.5 MHz as shown in Figure 6. The band-pass feature in every frequency bin was subtracted by calculating the mean across the phase bins, thus removing the broadband RFI. Figure 8 shows the phased pulse profile and the waterfall after median subtraction.

With the binning correlator we see a 9.02 dB detection of the pulsar. With a 4.20% duty-cycle of the pulsar (5 bins out of 119 bins have pulsar peak), and an integration time of 1.19 seconds (119 bins each with sub-integration of 10 ms), we get 267 integrations over all from the binning correlator output. Using this for LWA-1 auto-correlations from equation 6 we get an expected noise level of 320.21 mJy. The reported flux of B1133+16 is 4.73 ± 2.37 Jy, thus the expected SNR is $11.69^{+1.76}_{-3.02}$ dB. Table 2 gives the SNR estimated for LWA-1 correlated with a single VLA dish and with all of the 26 dishes. Keeping the bandwidth and integration time fixed, and with an approximate SEFD of 6000 Jy for the 40 m dish with LWA feed at its prime focus the SNR for the detection of B1133+16 was also estimated for cross correlation of OVRO-LWA with the 40 m dish.

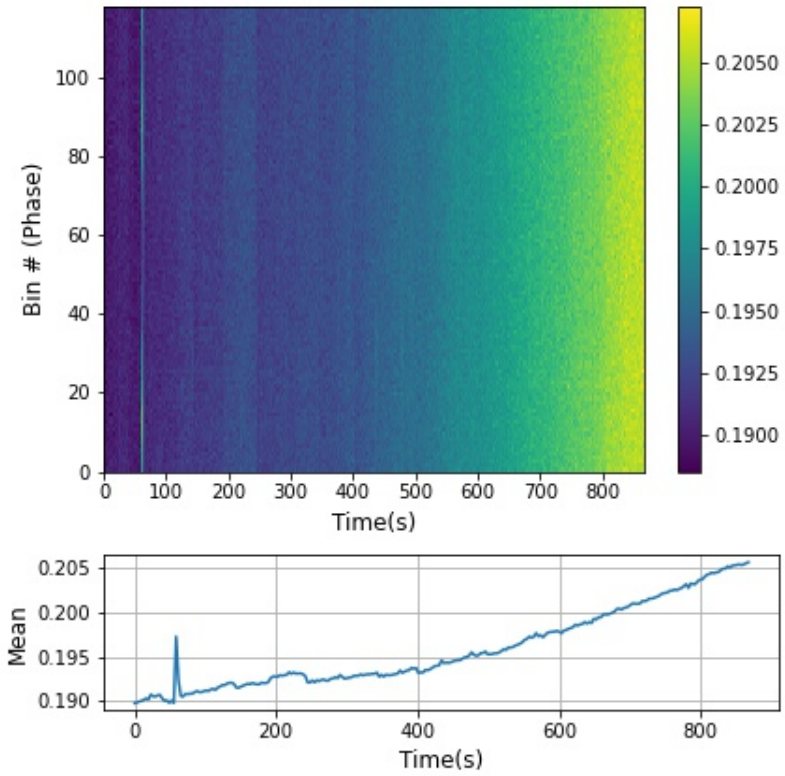

Figure 4. Autocorrelation products of LWA-1 from the binning correlator. The number of bins was set to 119, to match the pulse period in phase considering a fixed 10 ms sub-integration time of the binning correlator. The waterfall and the average across 119 bins clearly show a glitch at around ∼61 s.

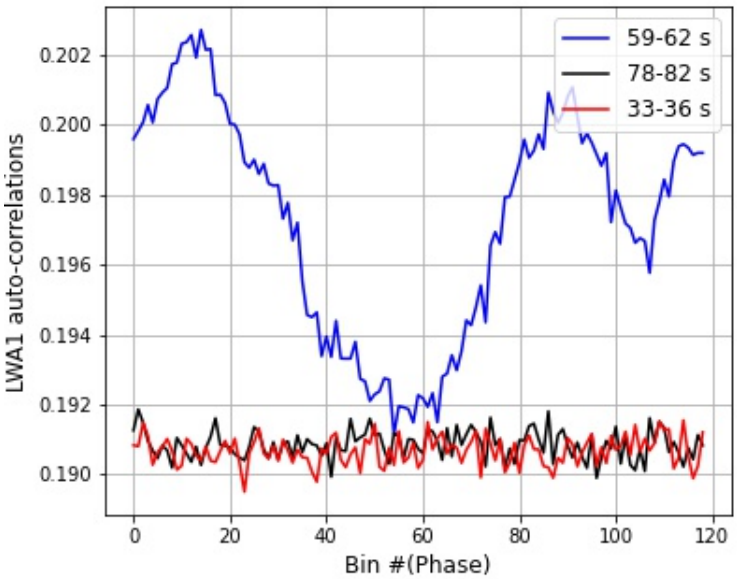

Figure 5. Glitch at ∼61 s in the auto-correlations of LWA-1, plotted alongside two other bins for reference.

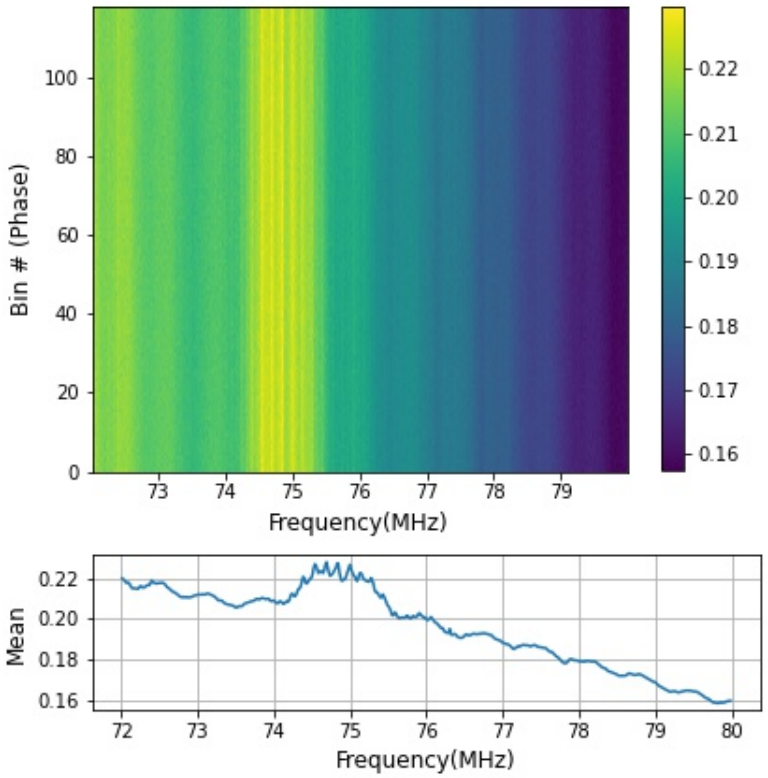

Figure 6. *(Top):* Waterfall of auto-correlation products of LWA-1 from the binning correlator averaged across the time times. *(Bottom):* Average across the phase bins shows a band-pass feature and RFI in the frequency range of 74-75.5 MHz

Correlation Mode	SEFD	Expected SNR (dB)
LWA-1 Auto-correlation	4680 Jy	$11.69^{+1.76}_{-3.02}$
LWA-1 & VLA single dish	4680 Jy 50 kJy	$6.55^{+1.76}_{-3.02}$
LWA-1 & 26 VLA dishes	4680 Jy 1961 Jy	$13.58^{+1.76}_{-3.02}$
OVRO-LWA & 40m dish	4680 Jy 6000 Jy	$11.15^{+1.76}_{-3.02}$

Table 2. Expected SNR for three different correlation modes, estimated for the detection of pulsar B1133+16 of flux 4.73 ± 2.37 J. SNR is also estimated for cross correlation of OVRO-LWA and the 40 m dish with LWA feed at its prime focus, assuming an approximate SEFD of 6000 Jy.

4. CONCLUSION

In this project, we propose using simultaneous observations of a bright pulsar tracking with VLA and letting it drift through LWA to make beam measurements of LWA. We performed initial sensitiv-

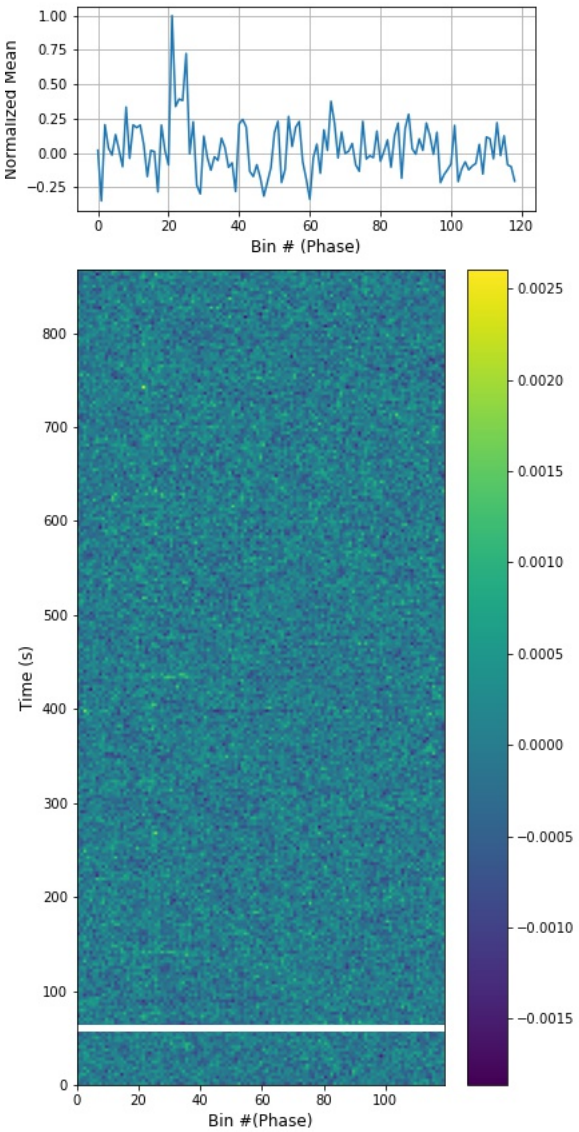

Figure 7. *(Top):*Time averaged pulse profile as seen in LWA-1 auto-correlations. *(Bottom):* Waterfall of LWA-1 auto-correlations.

ity analysis for LWA and VLA in different correlation modes and selected B1133+16 as a candidate pulsar. We recorded the data for bandpass and gain calibrators sources along with the target pulsar in eLWA mode for initial demonstration of the proof of concept. Despite the initial software and technical issues, we were able to detect the pulsar in LWA-1 auto-correlations using `PRESTO` with an SNR of 10.93 dB and using eLWA offline binning correlator with a 9.02 dB confidence. Both of these detections fall right within our expectation limits for B1133+16 of $11.69^{+1.76}_{-3.02}$ dB.

5. FUTURE WORK

This is a work in progress and has several areas of improvement and development. The next step in the project is to calibrate the data, check the gain stabilities and apply the calibration solutions to the pulsar to calculate absolute flux, which can be used to calculate the beam of LWA-1. We then plan to select at least two other bright sources to demonstrate the feasibility of the proposed

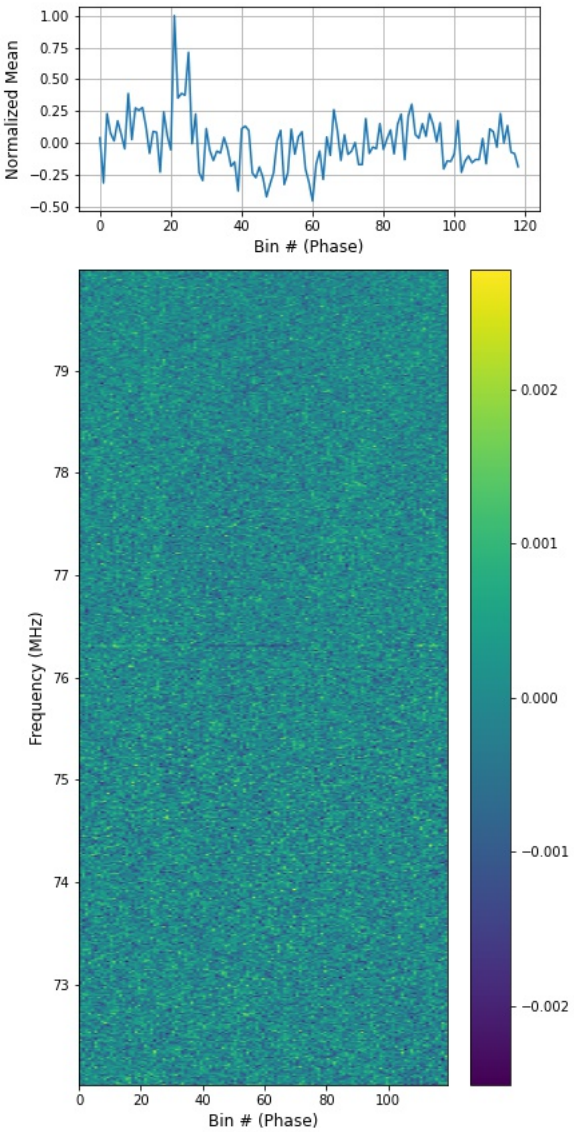

Figure 8. *(Top):*Frequency averaged pulse profile as seen in LWA-1 auto-correlations. *(Bottom):* Waterfall of LWA-1 auto-correlations.

methodology for VLA-LWA system. A long term objective is to make a similar beam measurement of OVRO-LWA using the 40 m dish at OVRO with an LWA feed installed at it's prime focus. We also plan to potentially set up a pipeline to periodically repeat these beam measurements as required.

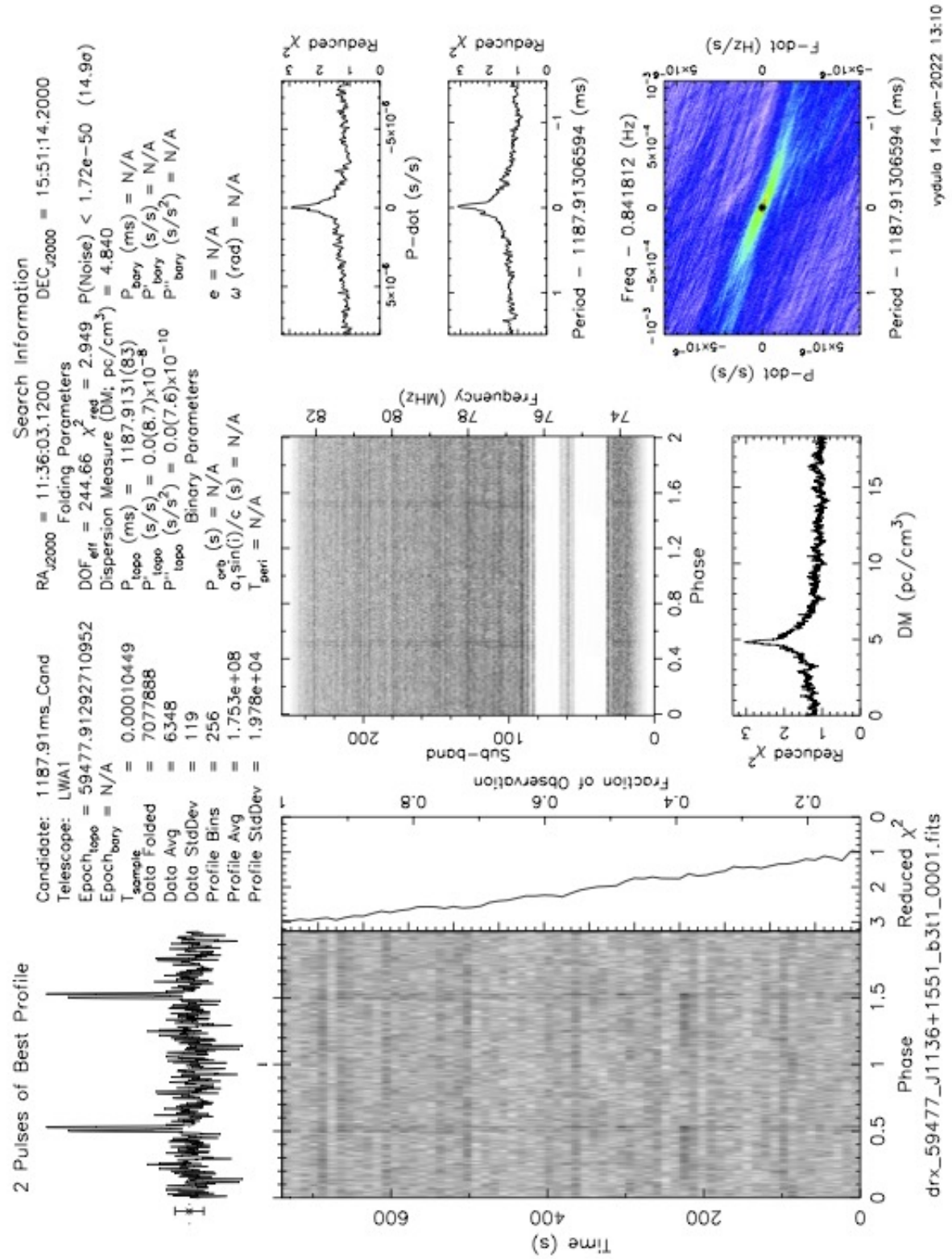

Figure 9. PRESTO's 14.9σ (10.93 dB) detection of B1133+16 using data recorded by LWA-1. *(Top left)* phased pulse profile showing a double peak, *(Bottom-left)* Phased waterfall against the scan duration and a reduced χ^2 measured for a random noise model, *(Top-middle)* phased waterfall against frequency, also showing the applied RFI masks, *(Bottom-middle)* best-fit DM *(Right)* best-fit period derivative ($P - dot$), best-fit period (P) and a $P - vs - P - dot$.

REFERENCES

Abdurashidova, Z., Aguirre, J. E., Alexander, P., et al. 2022, The Astrophysical Journal, 925, 221

Anderson, M. M., Hallinan, G., Eastwood, M. W., et al. 2018, The Astrophysical Journal, 864, 22

Barry, N., Beardsley, A., Byrne, R., et al. 2019, Publications of the Astronomical Society of Australia, 36

Barry, N., Bernardi, G., Greig, B., Kern, N., & Mertens, F. 2021, Journal of Astronomical Telescopes, Instruments, and Systems, 8, 011007

Berger, P., Newburgh, L. B., Amiri, M., et al. 2016, in Ground-based and Airborne Telescopes VI, Vol. 9906, International Society for Optics and Photonics, 99060D

Bernardi, G., De Bruyn, A., Brentjens, M., et al. 2009, Astronomy & Astrophysics, 500, 965

Bowman, J. D., Rogers, A. E., Monsalve, R. A., Mozdzen, T. J., & Mahesh, N. 2018, Nature, 555, 67

Burns, J., Hallinan, G., Chang, T.-C., et al. 2021, A Lunar Farside Low Radio Frequency Array for Dark Ages 21-cm Cosmology. https://arxiv.org/abs/2103.08623

Burns, J. O., Hallinan, G., Teitelbaum, L., et al. 2019a, "Probe Study Report: FARSIDE (Farside Array for Radio Science Investigations of the Darkages and Exoplanets", NASA. https://smd-prod.s3.amazonaws.com/science-red/s3fs-public/atoms/files/FARSIDE_FinalRpt-2019-Nov8.pdf.

Ciardi, B., Labropoulos, P., Maselli, A., et al. 2013, Monthly Notices of the Royal Astronomical Society, 428, 1755

Dowell, J., Wood, D., Stovall, K., et al. 2012, Journal of Astronomical Instrumentation, 1, 1250006

Ellingson, S. W. 2011, IEEE Transactions on Antennas and Propagation, 59, 1855

eLWA Observing Manual. 2021. https://science.nrao.edu/facilities/vla/docs/manuals/oss/performance/elwa

Furlanetto, S. R., Oh, S. P., & Briggs, F. H. 2006, Physics reports, 433, 181

Inoue, A. K., Tamura, Y., Matsuo, H., et al. 2016, Science, 352, 1559

Karuppusamy, R., Stappers, B., & Serylak, M. 2011, Astronomy & Astrophysics, 525, A55

Koopmans, L., Pritchard, J., Mellema, G., et al. 2015, arXiv preprint arXiv:1505.07568

Liu, A., & Shaw, J. R. 2020, Publications of the Astronomical Society of the Pacific, 132, 062001

LWA-1 Observing Manual. 2012, Sensitivity Analysis of LWA-1. http://lwa.phys.unm.edu/obsstatus/obsstatus006.html

Manchester, R. N., Hobbs, G. B., Teoh, A., & Hobbs, M. 2005, The Astronomical Journal, 129, 1993

Nambissan T, J., Subrahmanyan, R., Somashekar, R., et al. 2021, arXiv e-prints, arXiv

Newburgh, L. B., Addison, G. E., Amiri, M., et al. 2014, in Ground-based and Airborne Telescopes V, Vol. 9145, SPIE, 1709–1726

NRAO-VLA Observing manual. 2021, Exposure and overhead. https://science.nrao.edu/facilities/vla/docs/manuals/propvla/determining#section-3

Parsons, A. R., Liu, A., Aguirre, J. E., et al. 2014, The Astrophysical Journal, 788, 106

Price, D., Greenhill, L., Fialkov, A., et al. 2018, Monthly Notices of the Royal Astronomical Society, 478, 4193

Pritchard, J. R., & Loeb, A. 2012, Reports on Progress in Physics, 75, 086901

Ransom, S. M., Cordes, J. M., & Eikenberry, S. S. 2003, The Astrophysical Journal, 589, 911

Santos, M. G., Cooray, A., & Knox, L. 2005, The Astrophysical Journal, 625, 575

Singh, S., Nambissan, T., Subrahmanyan, R., et al. 2022, Nature Astronomy, 1

Spinelli, M., Bernardi, G., & Santos, M. 2018, Monthly Notices of the Royal Astronomical Society, 479, 275

Stovall, K., Ray, P., Blythe, J., et al. 2015, The Astrophysical Journal, 808, 156

Taylor, G. B., Carilli, C. L., & Perley, R. A. 1999, Synthesis Imaging in Radio Astronomy II, 180

Thomas, R. M., Zaroubi, S., Ciardi, B., et al. 2009, Monthly Notices of the Royal Astronomical Society, 393, 32

Windhorst, R. A., Cohen, S. H., Jansen, R. A., Conselice, C., & Yan, H. 2006, New Astronomy Reviews, 50, 113

Yatawatta, S., De Bruyn, A., Brentjens, M. A., et al. 2013, Astronomy & Astrophysics, 550, A136

APPENDIX

A. OBSERVING SEQUENCE

Source	Time	Comments
–	9 min	Dummy Slew
Cygnus-A	30 s	Set-up slew
Cygnus-A	5 min	Band-pass calibrator
–	3 min	Slew on 3C196
3C196	10 s	Gain set-up & resetting requantizers
3C196	5 min	Secondary Calibrator
3C295	8 min	Primary Calibrator
B1133+16	15 min	Target pulsar (10 Hz switched power disabled)
3C295	7 min	Primary Calibrator
Total	53 min	LST window: 13.5 h to 15 h

Table 3. Observation sequence in eLWA mode with two LWA stations and VLA 4-band system in B configuration, as recorded on September 20, 2021.